Photoacoustics 17 (2020) 100152

Contents lists available at ScienceDirect

Photoacoustics

journal homepage: www.elsevier.com/locate/pacs

Three-dimensional label-free imaging of mammalian yolk sac vascular remodeling with optical resolution photoacoustic microscopy

Doudou Huang[a,1], Yali Huang[b,1], Qi Qiu[b], Kai Wang[a], Zhihong Li[a], Youliang Yao[a], Gang Liu[a], Qingliang Zhao[a,**], Xiaoyuan Chen[c,*]

[a] State Key Laboratory of Molecular Vaccinology and Molecular Diagnostics & Center for Molecular Imaging and Translational Medicine, School of Public Health, Xiamen University, Xiamen 361102, China
[b] Medical School, Xiamen University, Xiamen 361102, China
[c] Laboratory of Molecular Imaging and Nanomedicine, National Institute of Biomedical Imaging and Bioengineering (NIBIB), National Institutes of Health (NIH), Bethesda, Maryland 20892, United States

ARTICLE INFO

Keywords:
Optical-resolution photoacoustic microscopy
Embryo development
Visceral yolk sac vascular
Vascular remodeling
Vascular density

ABSTRACT

Vessel development in the yolk sac is important for the embryo development and the malfunction of which can lead to cardiac dysfunction, embryonic malformation and miscarriage. Although substantial emphasis has been placed on the yolk sac vascular remodeling, no detailed three-dimensional (3D) imaging and quantitative analysis of this process has been described. Herein, we explored the development of the vascular system in the visceral yolk sac (VYS) on E11.5, E12.5 and E13.5 mouse embryos using a home-built large field-of-view (FOV) optical-resolution photoacoustic microscopy (OR-PAM). The results showed that OR-PAM can be used as a label-free imaging tool for studying the 2D/3D morphology changes of the vascular system during organogenesis. In addition, after a quantitative analysis the results showed that the microvascular density in the VYS gradually reduced along with the embryo growth. Vascular density in the VYS of E11.5 mouse embryos was almost 6-fold than that of E13.5. Hovever, the averaged vessel diameter of the entire VYS membrane increased gradually with the development of embryos. This study suggests that OR-PAM is a potential tool for acquiring the hemodynamic parameters of mammalian embryos, which could be further used for studying diseases related with the vascular remodeling such as vascular malformations and heart defects.

1. Introduction

Vasculogenesis in the visceral yolk sac (VYS) is considered as the first phase of vessel development [1–3]. It is also important for the gas exchange and nutrient export between the mother and the embryo before the placenta starts to function [4–6]. Thus, characterizing the vessel structural changes in the VYS is important for a range of applications in developmental biology. The vessel development in the VYS is often divided into three steps: vasculogenesis, angiogenesis, and vascular remodeling. The vasculogenesis and angiogenesis happen in mouse embryos from E7.5 to E9.5. The vasculature changes in the yolk sac from E7.5 to E9.5 have been recorded by the time-lapse fluorescence microscopy [1,7]. However, there is no study for exploring the vascular system in the VYS in the later embryonic stages. Meanwhile, several conventional imaging techniques, including micro-magnetic resonance imaging (MRI), ultrasound (US) imaging, laser confocal microscopy (LCM), and optical projection tomography (OPT), have been applied to study the embryonic cardiovascular development [8–10]. However, these tools have their own drawbacks for imaging vessels in the VYS. The major limits of MRI are that it is time-consuming and has relatively low resolution [11]. US imaging can detect the large vessels in real-time but is still difficult to achieve cellular-resolution imaging of tissues [12]. Although the LCM can obtain the high spatial resolution images, it often requires exogenous fluorescent probes [8]. OPT is good for the 3D visualization of the vasculatures at a high resolution but requires a tissue fixation step, thus not suitable for imaging live

Abbreviations: OR-PAM, optical-resolution photoacoustic microscopy; VYS, visceral yolk sac; MAP, maximum amplitude projection; LSF, line spread function

* Corresponding author at: Laboratory of Molecular Imaging and Nanomedicine, National Institute of Biomedical Imaging and Bioengineering (NIBIB), National Institutes of Health (NIH), Bethesda, Maryland 20892, United States.
** Corresponding author at: State Key Laboratory of Molecular Vaccinology and Molecular Diagnostics & Center for Molecular Imaging and Translational Medicine, School of Public Health, Xiamen University, Xiamen 361102, China.
E-mail addresses: zhaoql@xmu.edu.cn (Q. Zhao), shawn.chen@nih.gov (X. Chen).
[1] These authors contributed equally to this work.

https://doi.org/10.1016/j.pacs.2019.100152
Received 26 September 2019; Received in revised form 25 November 2019; Accepted 9 December 2019
Available online 23 December 2019

embryos [10]. Therefore, traditional imaging techniques above are difficult to perform a label-free, high-resolution, in vivo imaging for studying the VYS vessel development. A high-resolution, high-contrast imaging technology is of significance for understanding the morphological changes of the vascular system during embryo development.

Photoacoustic imaging (PAI) can provide both high axial resolution comparable to the high-frequency ultrasound imaging and a high specificity of the optical imaging. In addition, the preferential absorption of visible and near-infrared light by hemoglobin allows the visualization of vasculature up to centimeter depths [13–19] using PAI. Photoacoustic microscopy (PAM) is a branch of PAI with the highest lateral resolution. In this study, we aim to study the feasibility of using a home-built reflection-mode optical-resolution PAM (OR-PAM) system to monitor the vessel remodeling in the VYS during different development stages of mouse embryos.

2. Materials and methods

2.1. OR-PAM imaging system and protocol

The experimental setup of the home-built OR-PAM system is illustrated in Fig. 1(a). A 532 nm diode-pumped solid-state pulse laser (532-1-40 V, Advanced Optowave, USA) with a pulse width lower than 1.8 ns and a repetition rate of 5 kHz is used for irradiation. The output beam is attenuated by a neutral density filter (NDC-50C-4M-A, Thorlabs, USA), and then split into two beams by a beam splitter. The major beam is first expanded and then coupled into a low-cost multimode fiber (MMF) (HSNRM32, Sun Telecom, China) by a fiber coupler. The other beam is delivered to a photodiode (DET 10A, Thorlabs, USA for synchronizing the data acquisition with the laser pulse and monitoring laser pulse energy fluctuations. The output light from the MMF is expanded again before being focused by an objective lens (RMS4X, 0.1NA, Thorlabs, USA). An optical-acoustic combiner is made with a 45° right-angle prism and a rhomboid prism (fused silica, custom-made, Edmund Optics, USA). As shown in Fig. 1(b), the two prims are combined in a 3D-printed combiner with a thin layer of silicone oil being maintained at the interface between the two prisms. An ultrasound transducer (V214-BB-RM, central frequency: 50 MHz, -6 dB bandwidth: 70 %, Olympus, Japan) is attached on the rhomboid prism for photoacoustic (PA) signal detection. The detected PA signals are amplified by two amplifiers (ZFL-500, Mini Circuits, USA) and then acquired using a high-speed digitizer acquisition card (CompuScope 14200, Gage; Lockport, Illinois, USA) with a sampling rate of 200 MS/s. An acoustic lens (AL) (45–380, acoustic NA = 0.50, Edmund Optics, USA) is attached at the bottom of the rhomboid prism for acoustic focusing. The distance between the AL and the imaging plane is around 9 mm. In the experiment the AL is immersed in a water tank filled with ultra-pure water. The bottom of the water tank is a transparent high-density

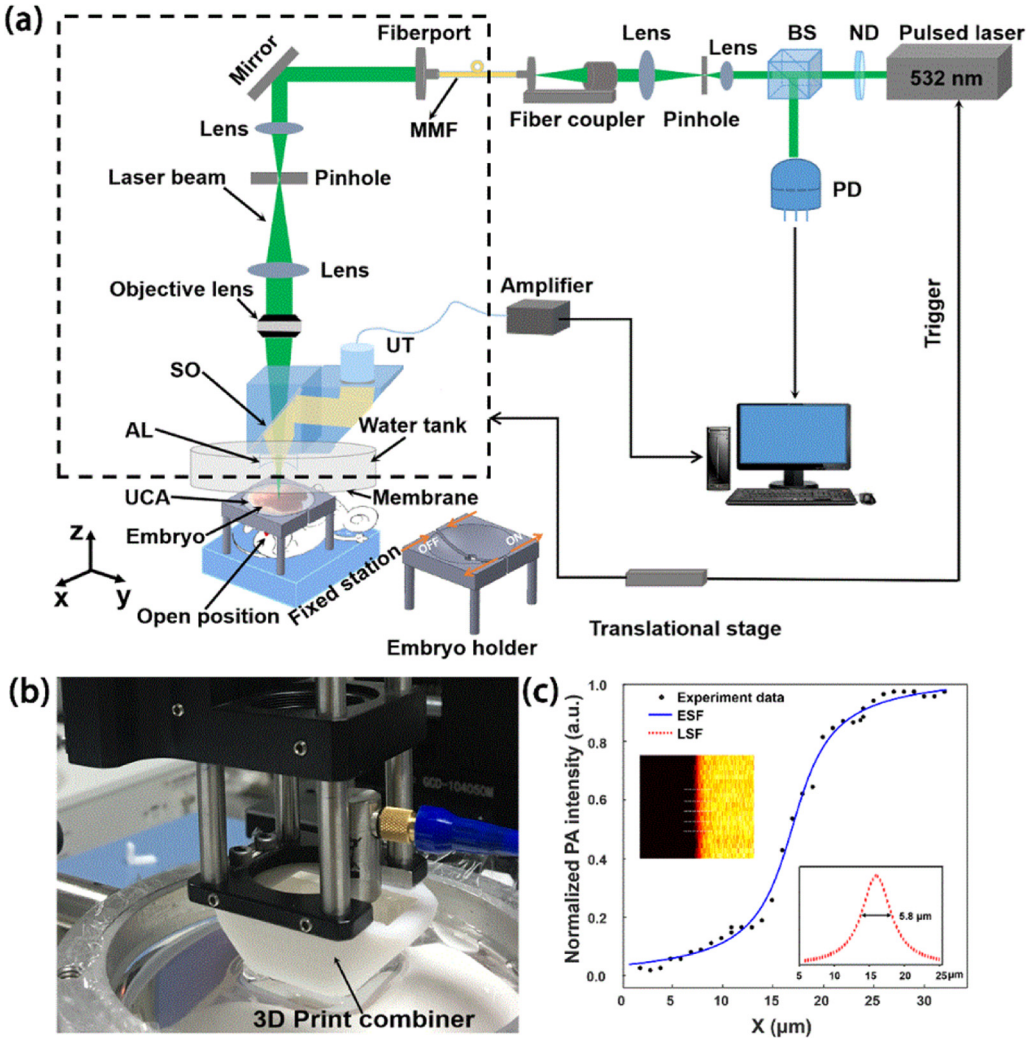

Fig. 1. (a) Schematic of the OR-PAM system for in vivo imaging the VYS of mouse embryos; (b) A photograph of the scan head; (c) Calibration of the system lateral resolution. BS: beam splitter; ND: neutral-density filter; MMF: multimode fiber; PD: photodiode; SO: silicone oil; AL: acoustic lens; UT: ultrasonic transducer. UCA: ultrasonic coupling agent.

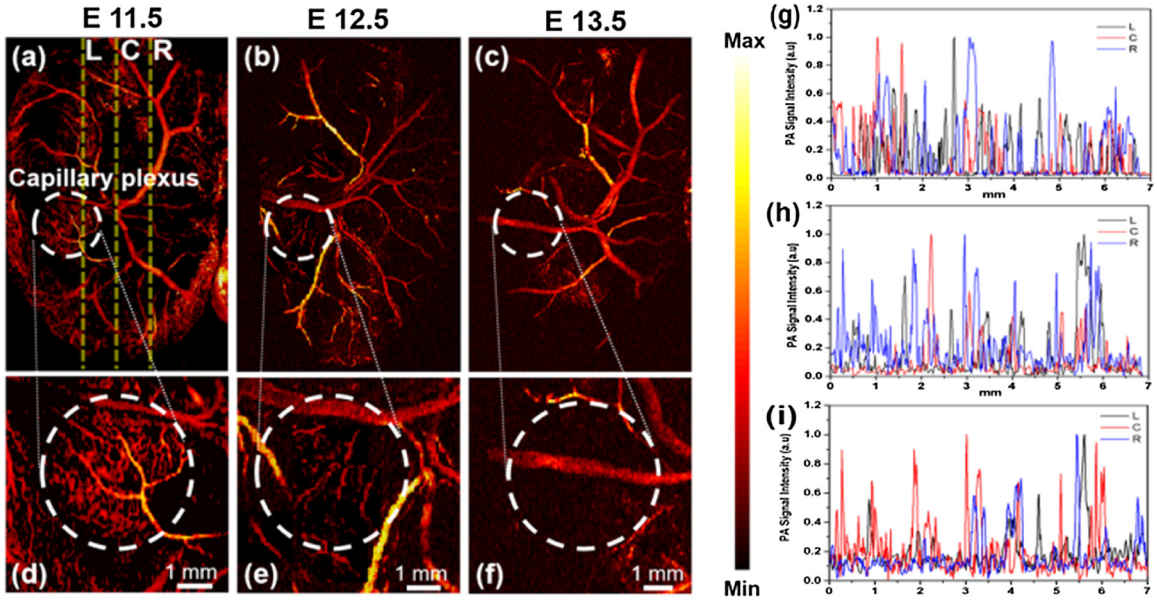

Fig. 2. Vessel development in the VYS of mouse embryos. (a–c) Representative PA MAP images showing the vascular system in the VYS at E11.5, E12.5 and E13.5, respectively. (d–f) Magnifications of the regions within the white circles at (a–c). (g–i) Normalized signal intensity profiles of the vessels along the yellow lines in (a–c). L: left; C: centerline; R: right.

polyethylene membrane. The ultrasonic coupling agent (UCA) is used between the film and the imaged sample. All the components within the dashed box in Fig. 1(a) are mounted on a two-dimensional (2D) translation stage (GCD-0310 M, Daheng optics, Beijing, China) to create raster-scanned images. To test the lateral resolution of the system, the edge of a razor blade was imaged and an edge-spread function was obtained by 5-times averaging, as shown in Fig. 1(c). The line-spread function (LSF) was derived from the ESF and the lateral resolution was measured to be 5.8 μm by measuring the full width at half maximum of the LSF. Compared with the theoretical lateral resolution of 2.7 μm, the actual resolution is slightly worse, which is probably due to the optical aberration at the coupling interfaces between the two prisms, as well as between the rhomboid prism and the AL. The used laser pulse energy on the tissue surface is ~ 400 nJ. The measured half angle of the focused beam after the objective lens was ~13.6°. By adjusting the optical focus at ~ 0.1 mm below the tissue surface, the surface laser fluence can be estimated as ~22 mJ/cm^2 [= (400 nJ)/(π × ((0.1 mm) ×tan (13.6°))^2)], which is slightly over the safety limit defined by ANSI standards (Laser Institute of America, American National Standard for Safe Use of Lasers ANSI Z136. New York, NY: American National Standards Institute Inc; 2007). To ensure that all the embryos remain in a good physiological state, the surfaces of the embryos were covered with normal saline. The embryos were exposed from the pregnant mice and all the embryos were alive during and after imaging, as their heart beats were clearly observed and recorded after the experiment (Supporting Information: Video 1). The embryos were sacrificed after the experiment.

2.2. *In vivo imaging process and experimental design*

In the *in vivo* experiments were conducted on three groups (E11.5, E12.5 and E13.5) with each group containing three or more embryos (n ≥ 3) from the same pregnant mouse to reduce the impact of individual differences. The Institute of Cancer Research outbred mouse line (ICR) mouse embryos were collected at specific aforementioned developmental stages. Timed mating was set up overnight. Noon on the day of finding a vaginal plug was designated as E0.5. Details about the breeding of pregnant mice were described in our previous study [20]. During the whole imaging process, the pregnant mouse was anesthetized with isoflurane (2 %; RWD Life Science, Shenzhen, China). A heating pad was utilized to maintain the temperature of the embryos. The belly skin of the pregnant mouse was cut open about ~1 cm, and the embryo was pushed through this opening and exposed for imaging. The myometrium of the embryo was carefully cut apart and then the entire embryo with intact yolk sac membrane and placenta was exposed. Phosphate buffered saline was used to remove residual blood from the VYS membrane surface quickly. During imaging, the embryo was fixed in a home-made embryo holder to reduce the minor movement. Meanwhile, to keep the embryo alive, the embryos were not dissected from the uterus. Instead, we cut a small gap in the myometrium to expose the yolk sac of the embryo but with the umbilical cord and placenta completely connecting to their mothers. The exposed embryo was kept in a home-built adjustable (OFF-ON) holder to fit in with the size of the embryo as shown in Fig. 1(a) (the inset: embryo holder). After recording the patterns of the vessels in the VYS at a specific stage, the mice were sacrificed and the embryos were harvested. All the animal experimental procedures were approved by the Institutional Animal Care and Use Committee of Xiamen University. Image processing and vascular quantification were analyzed using the developed algorithm implemented in MATLAB (R2017, The Mathworks, Natick, MA, USA) as described previously [21].

3. Results and discussion

The mouse embryo is an important model for studying the morphogenetic changes of the vessel development. To demonstrate the imaging ability of our OR-PAM system, the mouse embryo (a region of 7 mm × 9 mm) was imaged with a scanning step size of 20 μm at Y axis. Each imaging obtained 1000 × 450 scanning points and cost approximately 20 min. The imaging time is mainly determined by the repetition rate of the laser and the speed of the scanning stage. The results are presented in Fig. 2(a–c) in the form of the maximum-amplitude-projection (MAP) images of different developmental stages (E11.5-E13.5). Fig. 2(d–f) are the magnified images of the white circles capillary plexus at Fig. 2(a–c). As we can see that the microvessels were most abundant at E11.5 in Fig. 2(d), however, the number of microvessels decreased at E12.5 in Fig. 2(e). The microvessels almost disappeared at E13.5 in Fig. 2(f). Moreover, the microvessels in the marginal areas were also reduced during the embryo growth in Fig. 2(a–c). The decrease in the vessel number might be related to the maturation of

the placenta. In mouse embryos, the placenta starts to fully function after E11.5 and takes over the responsibilities for delivering the oxygen and nutrition. The reduction of vessel numbers and vessel density from E11.5 to E13.5 could also be due to the redundancy of functions in the vascular system of the yolk sac and the fusion of the vessels [22]. It has been shown previously that the small vessels could fuse to large major vessels in the yolk sac [23]. In the present study, we might miss some capillaries with the Y-axis scanning step size of 20 μm. However, this step size cannot be further reduced as embryos were highly dependent on the *in vivo* environment and would die if longer imaging time is applied. Furthermore, the capillaries were normally branched away from larger vessels. Therefore, missing some capillary distribution won't greatly influence the vessel pattern in the embryos at different stages.

For a better understanding of the changes of PA signals in VYS microvascular changes, we chose another two positions, 1.5 mm from the centerline in either direction (three yellow lines in Fig. 2(a)) for vascular quantification analysis through comparing the differences of PA signals among the three developmental stages. The overall trends are shown in Fig. 2(g–i). Normalized PA signals induced by microvasculature at E11.5 are denser than those of E12.5 and E13.5. As we can see, the number of the signal peaks reduced from E11.5 to E13.5 (Fig. 2(g–i)). This also demonstrates the reduction of the microvessel density during the embryo growth. Overall, the above results show that vessel remodeling in the VYS during development can be clearly imaged by OR-PAM. Moreover, the PA signals can properly demonstrate the change of the vascular density and architecture in the VYS.

In a further study, we investigated the vessel density and vessel diameter of VYS at three difference development stages. The overall flowchart of the vessel extraction algorithm was presented in Fig. S1 (Supporting Information). Briefly, as shown in Fig. S1, by using the original image, Hessian matrix feature map, binarized image, and vascular skeleton centerlines, the vessel parameters vessel density and vessel diameter can be extracted. More details of the vessel parameters calculation can be found in Refs. [24]. Fig. 3(a) is a representative original image of the vascular system in the VYS of an E12.5 embryo. The morphology of the microvasculature can be clearly observed in Fig. 3(a). Fig. 3(b) and (c) are the transverse and sagittal views of Fig. 3(a). The algorithm for quantifying the vessels parameters first uses the median filter for smoothing and (3-by-3 neighborhood size) suppressing noise. And then, in order to achieve enough contrast for smaller blood vessels, we performed intensity modification on the preliminarily processed image. The details of the intensity transformation calculation can be found in Refs. [24–26]. The remaining steps of the algorithm are described by using a representative region in the white dashed box in Fig. 3(a). Fig. 3(d) is the Hessian matrix feature map, as shown in the comparison of the image in the white dashed boxes in Fig. 3(a). The Hessian matrix-treated images show a higher image contrast and more uniform intensity distribution within the blood vessels than the original image (Fig. 3(a)). The optimal value of the threshold was automatically calculated by Otsu's method depending on gray value distribution of image. Subsequently a traditional region-based image segmentation method was utilized to process the binary images [27]. Vascular skeletons and vessel centerline were then extracted by a multi-stencils fast marching (MSFM) methods [28,29]. Fig. 3(e) shows the results of extracted microvessels overlaid with the vessel centerlines. The gray lines represent the calculated centerlines, and the blue regions represent the extracted vessels. For quantification, we then calculated the vessel density and vessel diameter of the VYS at different developmental stages in Fig. 3(f) and (g).

The total microvessel density (MVD) is defined as the total length of the vessel per unit volume, as given below [24,25]:

$$MVD = \frac{TotalVesselLength}{ObservedVolume} \tag{1}$$

As we can see, the total vessels density significantly decreased from E11.5 to E13.5 in Fig. 3(f). Moreover, at E13.5 the total density of the vessels was only 1/6 that of E11.5 (Fig. 3(f)). These results demonstrate that OR-PAM can be used for 3D imaging of the dynamic process of the vascular system, and the vascular extraction algorithm is able to extract abundant vessel information for a quantitative analysis. Furthermore, the vessel diameter is another important parameter for assessing the VYS vascular development. Briefly, a normal line vertically through the vascular skeleton centerline intersects the vessel edges at two intersection points, and the distance between the two intersection points is defined as the vessel diameter of each specified point. More details of microvascular parameters quantification algorithm can be found in previous work [24,28]. From Fig. 3(g), we found that averaged vessel

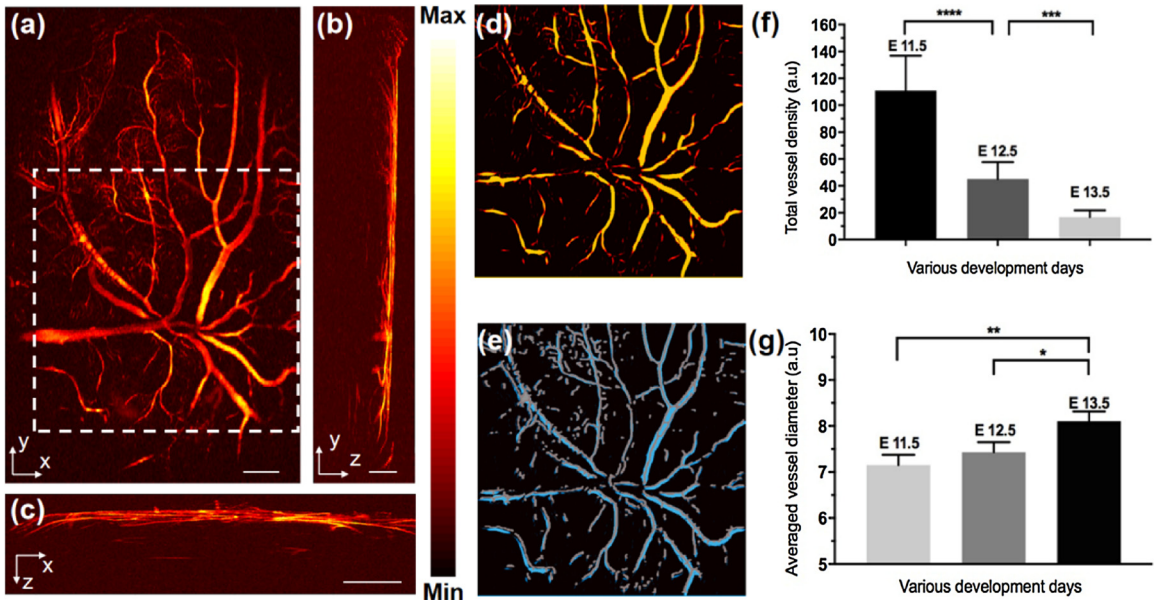

Fig. 3. Representative OR-PAM label-free triple-view VYS of an embryo at E12.5. (a), (b), and (c) refer to coronal, transverse, and sagittal planes of VYS microvascular, respectively; a representative region in the white dashed boxes to illuminate the dealing process of image in Fig. 3(a). (d) feature map after the Hessian matrix treated; (e) extracted microvessels binarized image overlaid with the vessel centerlines image. (f) and (g) statistical analysis of vessel density and vessel diameter in VYS of embryo at three different development stages, respectively. Bar: 1 mm in (a) and (c), 500 μm in (b).

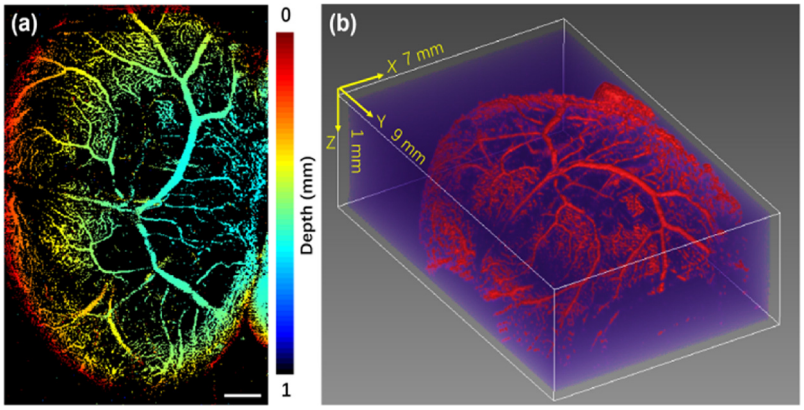

Fig. 4. Representative OR-PAM images of vascular system in the VYS at E11.5 acquired at 532 nm wavelength in vivo. (a) Depth-encoded top-view MAP images of the vascular system in VYS membrane. (b) 3D volumetric rendering of the vascular system in the VYS. Bar: 1 mm.

diameter of the entire VYS membrane increased gradually with the development of embryos. This phenomenon is probably attributable to the fusing of smaller vessels to form large major vessels as an adjustment to the demands of the expanding yolk sac and growing embryo [30].

Fig. 4(a) shows a depth-encoded MAP vasculature image in the VYS at E11.5. The color scale represents depth along z axis below the yolk sac surface. Fig. 4(b) shows a 3D volumetric rendering of the VYS vascular system. As can be seen, most microvessels close to the vitelline artery are normally located in the deeper region of the VYS at E11.5, as shown in Fig. 4(a) and (b). Moreover, the large blood vessels are mainly located in the center of the YVS. These results suggest that OR-PAM is a potential tool for detecting vessel remodeling in mammalian embryos. As the vessel development and remodeling on the yolk sac is closely related to the cardiac function [31,32], many genetic mutants with cardiovascular deficiency are found to have abnormalities on the VYS. Our study findings may have important implications for understanding how vessel system in the VYS functions and supports the growth of the embryo.

However, there are also several limitations in this study. For example, the mechanisms for the vessel remodeling at these developmental stages are still not clear. Some studies showed that the vessel remodeling is dependent on hemodynamic force due to direct endothelial cell migration and vessel fusion events. A study using time-lapsed confocal microscopy also showed that smaller vessels fuse to form the large major vessels of the yolk sac from E8.5 to E9.5 [7]. Therefore, considerably more work will need to be done to determine the relationship of vessel remodeling in the VYS and the embryo growth. Meanwhile, in this work, a single wavelength laser was used for structural imaging of blood vessels. In the future studies, multi-wavelength lasers could be used for functional imaging of VYS to extract further information such as the oxygenation saturation of these blood vessels.

4. Conclusion

In summary, to our best knowledge, this is the first time the OR-PAM is applied for label-free imaging and quantitative analysis of the VYS development on living mouse embryos. Our results show that OR-PAM is capable of label-free live imaging of the vessel development and vascular remodeling process at different developmental stages. Based on the detailed 3D live imaging of the yolk sac development from E11.5 to E13.5, we found that the number of vessels, the total length and the vessel density of the VYS gradually decreased from E11.5 to E13.5. Therefore, our study of vessel remodeling on the VYS may provide some indications for the assessment of cardiovascular functions in the embryos and could also be of benefit in the detection of congenital disease.

Declaration of Competing Interest

The authors declare that there are no conflicts of interest.

Acknowledgments

This work was supported by the Intramural Research Program, National Institute of Biomedical Imaging and Bioengineering, National Institutes of Health (ZIA EB000073), National Natural Science Foundation of China (NSFC) (81701743), Xiamen Science and Technology Plan Project (3502Z20183018), the Scientific Research Foundation of State Key Laboratory of Molecular Vaccinology and Molecular Diagnostics. (2017KF05, 2017KF06), National Science Foundation of Fujian Province of China (13171093), Fundamental Research Funds for the Central Universities of China (20720160118) and the Fujian Provincial Health Education Joint Research Project (WKJ2016-2-20).We would like to thank Professor Hao-Li Liu, Department of Electrical Engineering, Chang Gung University, for discussing the project.

Appendix A. Supplementary data

Supplementary material related to this article can be found, in the online version, at doi:https://doi.org/10.1016/j.pacs.2019.100152.

References

[1] M.D. Garcia, I.V. Larina, Vascular development and hemodynamic force in the mouse yolk sac, Front. Physiol. 5 (2014) 308.
[2] M.H. Baron, Embryonic origins of mammalian hematopoiesis, Exp. Hematol. 31 (2003) 1160–1169.
[3] J. Palis, M.C. Yoder, Yolk-sac hematopoiesis: the first blood cells of mouse and man, Exp. Hematol. 29 (2001) 927–936.
[4] C. Freyer, M.B. Renfree, The mammalian yolk sac placenta, J. Exp. Zool. B Mol. Dev. Evol. 312 (2009) 545–554.
[5] A.M. Carter, A.C. Enders, Placentation in mammals: definitive placenta, yolk sac, and paraplacenta, Theriogenology 86 (2016) 278–287.
[6] W.P. Jollie, Development, morphology, and function of the yolk-sac placenta of laboratory rodents, Teratology 41 (1990) 361–381.
[7] J.L. Lucitti, E.A. Jones, C. Huang, J. Chen, S.E. Fraser, M.E. Dickinson, Vascular remodeling of the mouse yolk sac requires hemodynamic force, Development 134 (2007) 3317–3326.
[8] M.H. Malone, N. Sciaky, L. Stalheim, K.M. Hahn, E. Linney, G.L. Johnson, Laser-scanning velocimetry: a confocal microscopy method for quantitative measurement of cardiovascular performance in zebrafish embryos and larvae, BMC Biotechnol. 7 (2007) 40.
[9] J.A. Ketterling, O. Aristizabal, B.Y.S. Yiu, D.H. Turnbull, C.K.L. Phoon, A.C.H. Yu, R.H. Silverman, High-speed, high-frequency ultrasound, in utero vector-flow imaging of mouse embryos, Sci. Rep. 7 (2017) 16658.
[10] G.A. Anderson, M.D. Wong, J. Yang, R.M. Henkelman, 3D imaging, registration, and analysis of the early mouse embryonic vasculature, Dev. Dyn. 242 (2013) 527–538.
[11] B.J. Nieman, N.A. Bock, J. Bishop, X.J. Chen, J.G. Sled, J. Rossant, R.M. Henkelman, Magnetic resonance imaging for detection and analysis of mouse phenotypes, NMR Biomed. 18 (2005) 447–468.

[12] P. Pallares, M.E. Fernandez-Valle, A. Gonzalez-Bulnes, In vivo virtual histology of mouse embryogenesis by ultrasound biomicroscopy and magnetic resonance imaging, Reprod. Fertil. Dev. 21 (2009) 283–292.
[13] L.V. Wang, S. Hu, Photoacoustic tomography: in vivo imaging from organelles to organs, Science 335 (2012) 1458–1462.
[14] R. Cao, J. Li, B. Ning, N. Sun, T. Wang, Z. Zuo, S. Hu, Functional and oxygen-metabolic photoacoustic microscopy of the awake mouse brain, Neuroimage 150 (2017) 77–87.
[15] M. Liu, N. Schmitner, M.G. Sandrian, B. Zabihian, B. Hermann, W. Salvenmoser, D. Meyer, W. Drexler, In vivo three dimensional dual wavelength photoacoustic tomography imaging of the far red fluorescent protein E2-Crimson expressed in adult zebrafish, Biomed. Opt. Express 4 (2013) 1846–1855.
[16] J. Laufer, F. Norris, J. Cleary, E. Zhang, B. Treeby, B. Cox, P. Johnson, P. Scambler, M. Lythgoe, P. Beard, In vivo photoacoustic imaging of mouse embryos, J. Biomed. Opt. 17 (2012) 061220.
[17] S. Hu, K. Maslov, L.V. Wang, Second-generation optical-resolution photoacoustic microscopy with improved sensitivity and speed, Opt. Lett. 36 (2011) 1134–1136.
[18] K.P. Kubelick, E.J. Snider, C.R. Ethier, S. Emelianov, Development of a stem cell tracking platform for ophthalmic applications using ultrasound and photoacoustic imaging, Theranostics 9 (2019) 3812–3824.
[19] R. Cao, J. Li, Y. Kharel, C. Zhang, E. Morris, W.L. Santos, R.L. Kevin, Z. Zuo, S. Hu, Photoacoustic microscopy reveals the hemodynamic basis of sphingosine 1-phosphate-induced neuroprotection against ischemic stroke, Theranostics 8 (2018) 6111–6120.
[20] Y. Huang, M. Li, D. Huang, Q. Qiu, W. Lin, J. Liu, W. Yang, Y. Yao, G. Yan, N. Qu, V.V. Tuchin, S. Fan, G. Liu, Q. Zhao, X. Chen, Depth-Resolved Enhanced Spectral-Domain OCT Imaging of Live Mammalian Embryos Using Gold Nanoparticles as Contrast Agent, Small 15 (2019) 1902346.
[21] Q. Li, L. Li, T. Yu, Q. Zhao, C. Zhou, X. Chai, Vascular tree extraction for photoacoustic microscopy and imaging of cat primary visual cortex, J. Biophoton. 10 (2017) 780–791.
[22] I.V. Larina, M.D. Garcia, T.J. Vadakkan, K.V. Larin, M.E. Dickinson, Imaging mouse embryonic cardiovascular development, Cold Spring Harb. Protoc. 10 (2012) 071498.
[23] R.S. Udan, J.C. Culver, M.E. Dickinson, Understanding vascular development, Rev. Dev. Biol. 2 (2013) 327–346.
[24] Z. Guo, Z. Li, Y. Deng, S. Chen, Photoacoustic microscopy for evaluating a lipopolysaccharide induced inflammation model in mice, J. Biophoton. 12 (2019) e201800251.
[25] Z. Yang, J. Chen, J. Yao, R. Lin, J. Meng, C. Liu, J. Yang, X. Li, L. Wang, L. Song, Multi-parametric quantitative microvascular imaging with optical-resolution photoacoustic microscopy in vivo, Opt. Express 22 (2014) 1500–1511.
[26] H. Zhao, G. Wang, R. Lin, X. Gong, L. Song, T. Li, W. Wang, X. Qain, H. Zheng, L. Li, Z. Liu, C. Liu, Three-dimensional Hessian matrix-based quantitative vascular imaging of rat iris with optical-resolution photoacoustic microscopy in vivo, J. Biomed. Opt. 23 (4) (2018) 046006.
[27] N.A. Otsu, Threshold selection method from gray-level histograms, IEEE Trans. Syst. Man Cybern. 9 (1979) 62–66.
[28] Q. Zhao, R. Lin, C. Liu, J. Zhao, G. Si, L. Song, J. Meng, Quantitative analysis on in vivo tumor-microvascular images from optical-resolution photoacoustic microscopy, J. Biophoton. 12 (2019) e201800421.
[29] M.S. Hassouna, A.A. Farag, Multistencils fast marching method: A highly accurate solution to the eikonal equation on cartesian domains, IEEE Trans. Pattern Anal. Mach. Intell. 29 (2007) 1563–1574.
[30] Q. Zhao, R. Lin, C. Liu, J. Zhao, G. Si, L. Song, J. Meng, Quantitative analysis on in vivo tumor-microvascular images from optical-resolution photoacoustic microscopy, J. Biophoton. 12 (2019) e201800421.
[31] J.K. Noveroske, L. Lai, V. Gaussin, J.L. Northrop, H. Nakamura, K.K. Hirschi, M.J. Justice, Quaking is essential for blood vessel development, Genesis 32 (2002) 218–230.
[32] M. Nisari, H. Ulger, E. Unur, O. Karaca, T. Ertekin, Effect of interleukin 12 (IL-12) on embryonic development and yolk sac vascularisation, Bratisl. Lek. Listy 115 (2014) 532–537.

Doudou Huang is now a master of school of public health and was enrooled at Xiamen University in 2018. She is interested in biomedical imaging, photoacoustic, optical coherence tomography and multi-modality molecular imaging technologies.

Assistant Professor Yali Huang teaching histology and embryology in the medical school of Xiamen University. She received her PhD degree from School of Biological Sciences, University of Edinburgh, UK in 2015. She is interested to understand the mechanism of habitual abortion and early developmental abnormalities of mammalian embryos.

Qi Qiu is a postgraduate of Xiamen university medical school, graduated from Harbin medical university in 2018 with a bachelor's degree. He is interested in neuroimaging of the brain.

Kai Wang is now a senior at Xiamen University. He is interested in the mechanism of tumorigenesis and targeted drugs for tumors.

Zhihong Li is currently an undergraduate at the school of public health at xiamen university, China. She is interested in biomedicine and studying hard in this direction. She will receive her undergraduate degree in 2020 and continue to study in this direction.

Youliang Yao is a master at Xiamen University and worked as an engineer in school of public health. He is interested in the mechanism of tumorigenesis and vaccinology.

Gang Liu received his MD degree from North Sichuan Medical College (China) in 2002 and PhD degree from Sichuan University (China) in 2009. Subsequently, He focused his training on nanomedicine and molecular imaging at the National Institutes of Biomedical Imaging and Bioengineering, National Institutes of Health. In 2012, he joined the Center for Molecular Imaging and Translational Medicine, Xiamen University. Currently he is a Full Professor of Biomedical and Bioengineering and his research interests include biomaterials, theranostics, and molecular imaging.

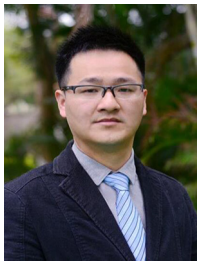

Qingliang Zhao is an Associate Professor at Xiamen University. He received his Ph.D degree from Shanghai Jiaotong University in Biomedical Engineering. His research focuses on biomedical optics, including photoacoustic, optical coherence tomography and multi-modality molecular imaging technologies.

Dr. Xiaoyuan (Shawn) Chen received his PhD in Chemistry from the University of Idaho. After two postdocs at Syracuse University and Washington University in St. Louis. He moved to NIH in 2009 and became a Senior Investigator and Chief of the Laboratory of Molecular Imaging and Nanomedicine (LOMIN) at the National Institute of Biomedical Imaging and Bioengineering (NIBIB), NIH. His current research interests include development of molecular imaging toolbox for better understanding of biology, early diagnosis of disease, monitoring therapy response, and guiding drug discovery/development.